

Synthesis of $\text{Al}_2\text{O}_3@\text{MnO}_2$ composite abrasives and their chemical mechanical polishing performance on silicon carbide (SiC)

Peijia Zhang^{a,b}, Hong Lei^{a,b,*}, Zefang Zhang^{c,d}, Jianhua Zhang^b, Shidong Chen^{b,e}, Xiaogang Hu^{a,b}

^a Research Center of Nano Science and Technology, College of Sciences, Shanghai University, Shanghai, 200444, China

^b Shanghai Engineering Research Center for Integrated Circuits and Advanced Display Materials, Shanghai University, Shanghai, 201899, China

^c School of Chemistry and Chemical Engineering, Shanghai University of Engineering Science, Shanghai, 201620, China

^d Shanghai Yingzhi Polishing Materials Co., Ltd., Qingpu District, Shanghai, 201700, China

^e School of Materials Science and Engineering, Shanghai University, Shanghai, 200444, China



ARTICLE INFO

Handling Editor: Dr P. Vincenzini

Keywords:

Composite abrasives

Chemical mechanical polishing (CMP)

Silicon carbide (SiC)

ABSTRACT

The effectiveness of silicon carbide (SiC) planarization mostly relies on the chemical and mechanical effects during chemical mechanical polishing (CMP). Nevertheless, the alumina (Al_2O_3) abrasive only provides a mechanical effect and is incapable of achieving a high-efficiency polishing of SiC. To address this issue, a series of novel $\text{Al}_2\text{O}_3@\text{MnO}_2$ composite abrasives were prepared by encapsulating varying amounts of manganese dioxide (MnO_2) on Al_2O_3 abrasive, and the polishing performance on SiC wafers was evaluated. The X-ray diffraction (XRD) and scanning electron microscope (SEM) images, along with the size and zeta potential data, show that MnO_2 is successfully coated on the surface of Al_2O_3 , and the dispersion of $\text{Al}_2\text{O}_3@\text{MnO}_2$ composite abrasive is significantly improved when compared with the pure Al_2O_3 . Furthermore, the CMP experiment and surface profile analysis demonstrate that the material removal rate (MRR) can reach a maximum value of 640.47 nm/h when using a 0.05 wt% MnO_2 -coated Al_2O_3 composite abrasive, which is 76 % higher than that of traditional Al_2O_3 abrasive. Furthermore, the average surface roughness (S_a , arithmetic mean height) of SiC is reduced to 0.73 nm. X-ray photoelectron spectroscopy results reveal that the surface of SiC is oxidized and forms a chemical bond known as Mn–O–Si after CMP. The results of the friction coefficient test and contact angle test indicate that slurries containing composite abrasive have exceptional wettability and a higher friction coefficient. Under the synergistic chemical and mechanical effects, SiC is oxidized to soft oxide and then removed circularly to reach excellent flatness.

1. Introduction

The third-generation semiconductor material silicon carbide (SiC) has better physical properties than traditional semiconductors, such as large band gap, high breakdown voltage, and high thermal conductivity. As a result, SiC is extensively utilized in high-frequency, high-power devices [1]. To attain widespread use, the epitaxial layer necessitates a SiC substrate that possesses a high-quality surface characterized by a surface roughness of less than 1 nm root mean square and an undamaged lattice structure [2]. Currently, chemical mechanical polishing (CMP) removes the rough peaks and defects on the surface of the materials through the synergistic effect of chemistry and machinery to obtain a high-precision smooth surface, so it has become the most effective

technology for global and local planarization of the wafer [3]. Due to the strong chemical inertness and the high hardness of the Si-face surface of SiC, the material removal rate (MRR) of the C-face surface is typically higher than that of the Si-face surface. Therefore, enhancing the MRR on the Si-face surface is a current research focus until mass production is accomplished [4].

It was found that the rate-limiting step in the total CMP process was the surface oxidation reaction of SiC [5]. Scholars have recently focused on utilizing oxidants to oxidize SiC into the transition oxidation state of Si–C–O, so that the mechanical effect of abrasive removes the soft oxide [6]. To achieve such an oxidation state of SiC, numerous researchers conduct scientific studies. Ni et al. [7] conducted a comparison of CMP performance on the Si surface of the 6H-SiC (0001) wafer using two

* Corresponding author. Research Center of Nano Science and Technology, College of Sciences, Shanghai University, China.

E-mail address: hong_lei2005@163.com (H. Lei).

strong oxidants, namely potassium permanganate (KMnO_4) and hydrogen peroxide (H_2O_2). Under identical pH conditions, H_2O_2 can undergo oxidation by KMnO_4 to produce O_2 , demonstrating that KMnO_4 have a greater capability for oxidation. The relative percentage content of chemical composition on the polished SiC surface was obtained. It was found that the oxidation product ($\text{Si}-\text{C}-\text{O}$ 、 $\text{Si}-\text{O}_x-\text{C}_y$ 、 $\text{Si}_4\text{C}_{4-x}\text{O}_2$ and $\text{Si}_4\text{C}_4\text{O}_4$) content of SiC polished by KMnO_4 is higher than polished by H_2O_2 . Chen et al. [8] investigated the use of colloidal silica and ceria-based slurries, together with KMnO_4 , to achieve a higher MRR in the CMP process of a 6H-SiC (0001) substrate. The results demonstrated that the smooth surface with the average surface roughness (Ra) of 0.11 nm and the large MRR of 1089 nm/h were attained in the strong acid environment. Wang et al. [9] studied the polishing characteristics of 4H-SiC (0001) using Al_2O_3 as an abrasive, KMnO_4 as an oxidant, and ferric nitrate as a chemical additive. The experiment demonstrated that adding 0.5 wt% ferric nitrate resulted in a 34% increase in the material removal rate of 4H-SiC compared with that without ferric nitrate. Additionally, the surface roughness Ra decreased from 0.123 nm to 0.110 nm. By analyzing the 2p spectrum of Si, it can be observed that in an acidic environment, the O atom only attacks the C atom and generates the $\text{Si}-\text{C}-\text{O}$ structure, but after adding ferric nitrate, the O atom attacks not only the C atom but also Si atom, generating SiO_2 and $\text{Si}-\text{O}_x-\text{C}_y$ structure. Zhao et al. [10] studied the high-quality polishing of SiC using manganese (Mn)-based slurry. In alkaline conditions, MnO_2 can be transformed into MnO_2^{2-} ions, which enhances the solid-phase chemical reaction at the interface, causes the oxidation reaction of the matrix's surface atoms, weakens the molecular bonds of SiC. Finally, the MRR is improved and the Ra reaches 1 nm. However, simply changing the composition of the slurry formula is not enough to effectively improve the MRR. As a result, it is possible to achieve SiC planarization by changing the structure of the abrasive.

Abrasive is one of the key factors in determining the quality of polishing, and Al_2O_3 abrasive hardness (the Mohs hardness is 9 [11]) is higher and more suitable for polishing hard and brittle materials such as SiC [12,13]. Su et al. [14] examined how the composition of the polishing slurry affects the MRR of SiC substrate based on Al_2O_3 abrasive in CMP. The polished surface can achieve a surface roughness of less than 1 nm. Nevertheless, Al_2O_3 abrasive has obvious disadvantages in CMP, such as excessive hardness and poor suspension stability and dispersion, which frequently lead to additional surface flaws [15]. Li et al. [16] used 2D layered zirconium phosphate (ZrP) and Al_2O_3 as hybrid abrasive, and polyethylene glycol (PEG) as a dispersant to prepare environment-friendly and efficient aluminum alloy CMP slurry. The dispersion stability was enhanced as a result of the hydrogen bond interaction between the hybrid abrasive produced by PEG. Simultaneously, Al_2O_3 , a widely used catalyst support material, has been coupled with other common nanomaterials to create diverse core-shell structures [17]. These structures find extensive applications in the field of CMP. Lei et al. [18] studied the CMP performance of $\text{Al}_2\text{O}_3/\text{SiO}_2$ core-shell abrasive on a hard disk matrix. The experiment revealed that the quantity of SiO_2 coating had a significant impact on the MRR. Additionally, the slurry with a core-shell structure exhibited lower surface roughness and fewer scratches compared to the slurry containing pure Al_2O_3 . Wang et al. [19] studied the CMP performance of Al_2O_3 -metatitanic acid composite abrasive with the core-shell structure on the sapphire substrate. The presence of a core-shell structure enhances both the surface quality and MRR due to the catalytic effect of the solid-phase chemical reaction occurring between metatitanic acid-coated Al_2O_3 and the sapphire substrate during the polishing process. Achieving an atomic surface with high MRR in CMP poses a difficulty due to the need to balance chemical and mechanical impacts [20]. Herein, certain academics aim to change the imbalance between chemical and mechanical impacts by modifying the quantity of coating on the shell in the core-shell structure. Their objective is to determine the ideal coating amount that yields the maximum MRR. Yuan et al. [21] synthesized a series of composite abrasives called zeolite imidazolium cerium oxide

($\text{CeO}_2@\text{ZIF-8}$) to enhance the concentration of Ce^{3+} . This was achieved by varying the quantity of zeolitic imidazolate framework (ZIF-8) material throughout the growth process. At a ZIF-8 concentration of 1.95 wt % in $\text{CeO}_2@\text{ZIF-8}$ composite abrasive, the MRR is 28% greater than that of pure ceria abrasive. Additionally, the average surface roughness (Sa), which measures the arithmetic mean height, is only 1.23 nm. Kurokawa et al. [22] achieved efficient CMP of SiC substrates by using MnO_2 slurry instead of silica slurry, adding the strong oxidant KMnO_4 , and introducing oxygen to increase the MRR. MnO_2 can be transformed into MnO_2^{2-} in a high pH environment, which existed in ionic form and has the advantage of being easier to react, promoting the oxidation process. Yin et al. [23] exploited the multi-valence and oxidation-reduction characteristics of MnO_2 particles to develop a new MnO_2 slurry for efficient and high-quality chemical mechanical polishing of SiC wafer. Experiments showed that MnO_2 particles were easily converted into MnO_2^- ions in alkaline environment, and the strong oxidation of MnO_2^- ions greatly improved the polishing efficiency. To summarize, Al_2O_3 , which is the most appropriate abrasive for SiC polishing, can be enhanced through structural innovation. MnO_2 , a common transition metal oxide catalyst, has garnered significant interest owing to its notable attributes including elevated catalytic activity, thermal stability, affordability, and facile production [24]. Hence, it can be deemed advantageous to amalgamate with Al_2O_3 in order to fabricate a novel form of composite abrasive.

Based on these studies, a novel $\text{Al}_2\text{O}_3@\text{MnO}_2$ core-shell structure nanocomposite abrasive that accelerates chemical reaction rate is prepared. This nanocomposite abrasive accelerates the pace of chemical reactions. By adjusting the amount of MnO_2 shell, the most suitable amount of coating to achieve the best CMP performance of SiC is found. The microstructure of $\text{Al}_2\text{O}_3@\text{MnO}_2$ composite abrasive was characterized by X-ray diffraction (XRD), scanning electron microscope (SEM), particle size distribution, CMP performance was tested by polishing experiment, three-dimensional optical profilometer, and polishing mechanism was analyzed by X-ray photoelectron spectroscopy (XPS), contact angle test and friction coefficient test.

2. Experiment

2.1. Chemicals

The Al_2O_3 abrasive was acquired from Shanghai Yingzhi Abrasive Materials Co., Ltd (China), potassium permanganate (KMnO_4), hydrochloric acid (HCl), and nitric acid (HNO_3) came from Sinopharm Chemical Reagent Co., Ltd (China). All reagents do not require further purification.

2.2. Preparation of $\text{Al}_2\text{O}_3@\text{MnO}_2$ composite abrasives

MnO_2 is grown on Al_2O_3 by a simple chemical deposition method. First, 15 g Al_2O_3 was added to 100 g deionized water, and an Al_2O_3 suspension was obtained after ultrasound for 25 min. To properly disperse the Al_2O_3 , a three-neck flask with the suspension was heated in a 50 °C water bath and magnetically agitated for 30 min. Then, 0.1669 g KMnO_4 and 5 mL 3 mol/L HCl were added to the Al_2O_3 dispersion and stirred. When dark brown solids appeared in the flask, the reaction stopped. Finally, the mixture was centrifuged at 5000 rpm for 5 min, washed three times continuously with deionized water and absolute ethanol, and dried at 60 °C for 12 h. The $\text{Al}_2\text{O}_3@\text{MnO}_2$ composite abrasive (the mass ratio of MnO_2 to Al_2O_3 is 0.50 wt%) was prepared, denoted as $\text{Al}_2\text{O}_3@\text{MnO}_2$ (0.50 wt%). To compare the impact of varying coating amounts on the polishing properties of $\text{Al}_2\text{O}_3@\text{MnO}_2$ composite abrasive, a series of $\text{Al}_2\text{O}_3@\text{MnO}_2$ composite abrasives with different contents of MnO_2 were prepared by changing the added amount of KMnO_4 in the above synthesis process. The mass ratio of MnO_2 to Al_2O_3 in these abrasives was 0.01 wt%, 0.03 wt%, 0.05 wt%, 0.1 wt%, 0.3 wt %, and 0.5 wt%, respectively. In addition, MnO_2 abrasive was prepared

by the same method as the reference. 0.1669 g KMnO₄ and 5 mL 3 mol/L HCl were added to 100g of deionized water to stir, and the reaction was stopped when dark brown substances appeared in the flask. The samples were centrifuged at 5000 rpm for 5 min, washed three times sequentially with deionized water and absolute ethanol, and dried at 60 °C for 12 h. Finally, MnO₂ abrasive is obtained.

2.3. Polishing performance test

The polishing experiment was carried out with 1.5 wt% Al₂O₃@MnO₂ composite abrasive. 6 g abrasive was added into 400 mL deionized water, while 4 g KMnO₄ was added as an oxidizer. The pH was adjusted with 3 mol/L dilute HNO₃ as a pH regulator, and the slurry was ultrasonic for 20 min. As a reference, pure Al₂O₃ polishing liquid was made using the same method.

A UNIPOL-1502 polishing machine (Shenyang Kejing Co., Ltd., China) was used to polish 4H-SiC (0001, the diameter of 2 inches, Shandong SICC Co., Ltd. China). The polishing pad was Suba 800 (Dow Chemical Co., Ltd., USA), and the setting parameters of polishing are shown in Table 1. Following the polishing process, SiC substrate was cleaned with acetone, cleaning agent, ethanol, and deionized water successively, dried in the oven at 60 °C for 30 min, cooled in the drying dish for 30 min, and then weighed. The formula for material removal rate (MRR) is as follows:

$$MRR = \frac{\Delta m * 10^4}{\rho \pi R^2 \tau}$$

Where, MRR: material removal rate (μ m/h); Δm : quality of SiC substrate removal before and after polishing (g); ρ : the density of SiC substrate (g/cm^3 , and $\rho_{\text{SiC}} = 3.16 \text{ g}/\text{cm}^3$); R: radius of SiC substrate (cm); τ : polishing time (h)

2.4. Characterization

The XRD patterns of Al₂O₃@MnO₂ composite abrasive was determined by Cu K α radiation by X-ray diffractometer (Rigaku, Japan). The operating voltage and current of the X-ray tubes were fixed at 40 kV and 40 mA, respectively. The scanning speed was set at 8° min^{-1} , and the step size was 0.02° . Intensity data were collected in the range of $20 = 20^\circ$ – 80° . The morphology of Al₂O₃ and Al₂O₃@MnO₂ composite abrasive was characterized by SEM (JSM-7500F, JEOL Ltd, Japan) at an accelerated voltage of 10.0 kV. Particle size distribution and Zeta potential test of Al₂O₃ and Al₂O₃@MnO₂ were determined by Nano ZS90 Zetasizer (Malvern Panalytical Ltd, UK). Before particle size and zeta potential testing, the abrasive was dispersed in deionized water. Different pH values of the system were adjusted with 0.1 mol/L NaOH and 0.1 mol/L HCl solutions, and tested after ultrasound for 10 min.

The mean surface roughness (Sa, arithmetic mean height) of SiC before and after polishing was measured by a three-dimensional optical profilometer (S neox 090, Sensofar S.L.). The pixel size was $0.69 \mu\text{m}/\text{pixel}$. The Z-scan was $596 \mu\text{m}$, and the measuring area was $500 \mu\text{m} \times 500 \mu\text{m}$. SiC surface before and after CMP was studied by XPS (Thermo Scientific K-Alpha, USA), and C1s peak was calibrated at 284.8 eV by focusing monochromatic Al K α radiation. The contact angle of slurry drops on SiC substrate surface was obtained by dynamic contact angle

and penetration analyzer (BIOLIN Theta Flex, Sweden). The experiment was repeated three times for each group. SiC polishing environment was simulated using a Byes-550 friction meter (Bangyi Precision Measuring Instrument Shanghai Co., Ltd., China.), and the friction coefficient between SiC substrate and the Al₂O₃ abrasive coated with different MnO₂ amounts was measured.

3. Results and discussion

3.1. Structure and morphology analysis of Al₂O₃@MnO₂ composite abrasive

3.1.1. XRD analysis

Fig. 1 is the XRD pattern of Al₂O₃@MnO₂ (0.50 wt%) composite abrasive. Pure MnO₂ (prepared in section 2.2) and Al₂O₃ abrasive were also evaluated as references. As shown in Fig. 2, MnO₂ has diffraction peaks at 25.7° , 37.5° , and $65.1^\circ(20)$ corresponding to the (220), (211), and (002) crystal faces, which are consistent with the α -MnO₂ image of the standard tetragonal system I4/m (PDF#44-0141) [25]. Al₂O₃@MnO₂ (0.50 wt%) composite abrasive has two kinds of diffraction peaks of MnO₂ and Al₂O₃. The Al₂O₃ peaks occur at the following angles: 25.6° , 35.2° , 37.8° , 43.4° , 46.2° , 52.5° , 57.5° , 59.7° , 61.3° , 66.5° , 68.2° and 76.9° . The peaks are sharp, strong, and exhibit good crystallinity, corresponding with the α -Al₂O₃ image of the standard tripartite system R3c (PDF#10-0173) [26]. The peaks of MnO₂ are at 25.7° , 37.5° , and 65.1° . The low intensity of the MnO₂ diffraction peak in Al₂O₃@MnO₂ may be due to the low content of MnO₂ and the weak crystallinity [27]. The XRD results show that MnO₂ and Al₂O₃ coexist in Al₂O₃@MnO₂ (0.50 wt%) composite abrasive, and MnO₂ is successfully synthesized on Al₂O₃.

3.1.2. SEM images, size distribution, and zeta position

To clearly demonstrate the typical morphology and dispersion of Al₂O₃ and Al₂O₃@MnO₂ (0.50 wt%) composite abrasive, SEM images were taken at the same multiples. Irregular polygonal Al₂O₃ abrasive is shown in Fig. 2a. The aggregation of Al₂O₃ abrasive is significant due to its high surface energy and van der Waals forces [28]. Fig. 2b shows the Al₂O₃@MnO₂ (0.50 wt%) composite abrasive. Due to the addition of MnO₂, the dispersion of Al₂O₃@MnO₂ (0.50 wt%) composite abrasive was significantly improved compared with pure Al₂O₃ abrasive [21]. The energy dispersion spectroscopy (EDS) results of region A of Al₂O₃ and region B of Al₂O₃@MnO₂ (0.50 wt%) composite abrasive are shown

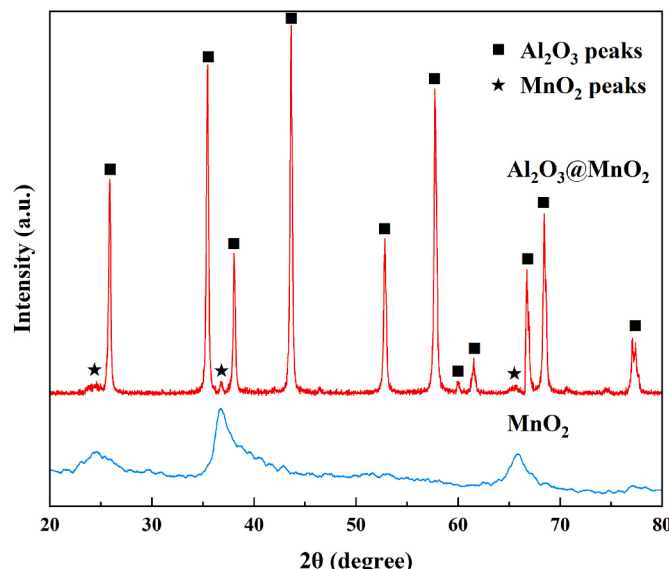


Fig. 1. XRD pattern of Al₂O₃@MnO₂ (0.50 wt%) and MnO₂ abrasives.

Table 1
Conditions of the polishing experiment.

Parameter	Value
Amount of slurry	400 mL
Abrasive concentration	1.5 wt%
pH	2
Polishing pad rotation speed	70 r/min
Load pressure	6 kg
Polishing time	1 h

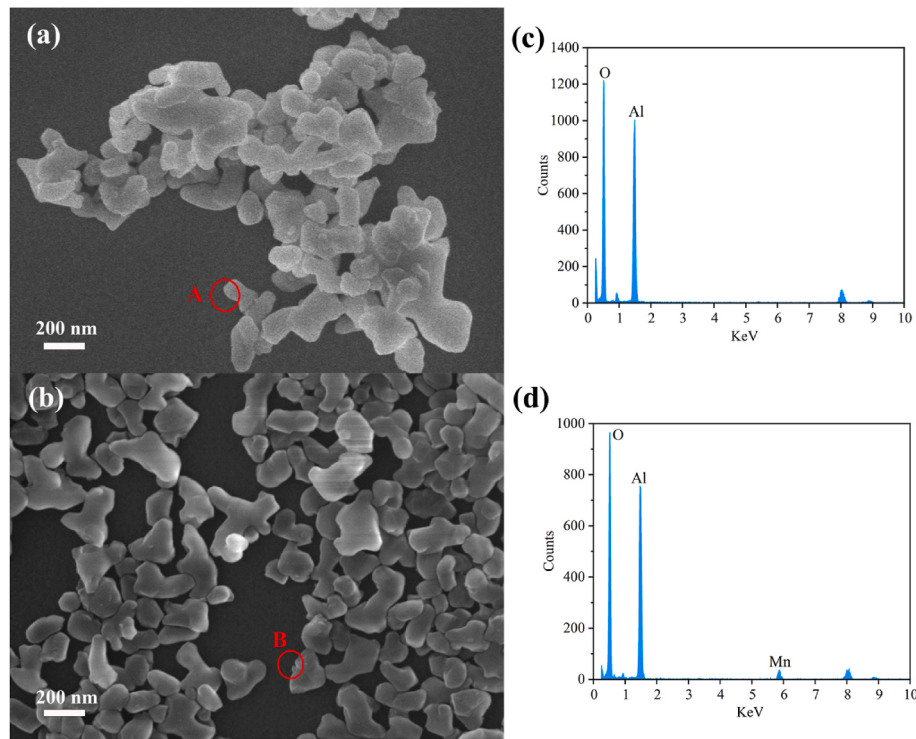


Fig. 2. SEM images of (a) Al₂O₃ and (b) Al₂O₃@MnO₂ (0.50 wt%) composite abrasive; EDS results of (c) region A of Al₂O₃ and (d) region B of Al₂O₃@MnO₂ (0.50 wt%) composite abrasive.

in Fig. 2c and d respectively. By comparison, the surface of MnO₂ coated Al₂O₃ (Fig. 2d) contains O, Al, and Mn components, whereas Al₂O₃ (Fig. 2c) does not exhibit any Mn peak. SEM and EDS image results confirmed the successful loading of MnO₂ on Al₂O₃, and the presence of MnO₂ improved the agglomeration of Al₂O₃@MnO₂ (0.50 wt%) composite abrasive.

Based on the literature, the formation of the hard agglomeration of abrasives in the polishing fluid may cause scratches on the substrate, so it is crucial to enhance the dispersion stability of abrasives [29]. Fig. 3 shows the particle size distribution of Al₂O₃ and Al₂O₃@MnO₂ composite abrasive with different MnO₂ contents at pH = 2. At coating amounts ranging from 0.01 wt% to 0.30 wt%, the sample exhibits a

narrow peak, and the particle size distribution of Al₂O₃@MnO₂ composite abrasive is narrower and smaller than that of pure Al₂O₃. When the coating amount is 0.5 wt%, the sample shows a wide peak. This indicates that adding an appropriate amount of MnO₂ on the abrasive can effectively alleviate the agglomeration phenomenon. This finding is consistent with the SEM results of the composite abrasive.

Furthermore, the zeta potential is closely related to the dispersion stability of the polishing slurry. When the absolute value of the zeta potential is greater than 30 mV, the stability of the polishing slurry improves as a result of the electrostatic repulsion between abrasive [30]. Fig. 4 shows the zeta potential of Al₂O₃ and Al₂O₃@MnO₂ (0.50 wt%) composite abrasive at different pH values. When pH is less than 6, the

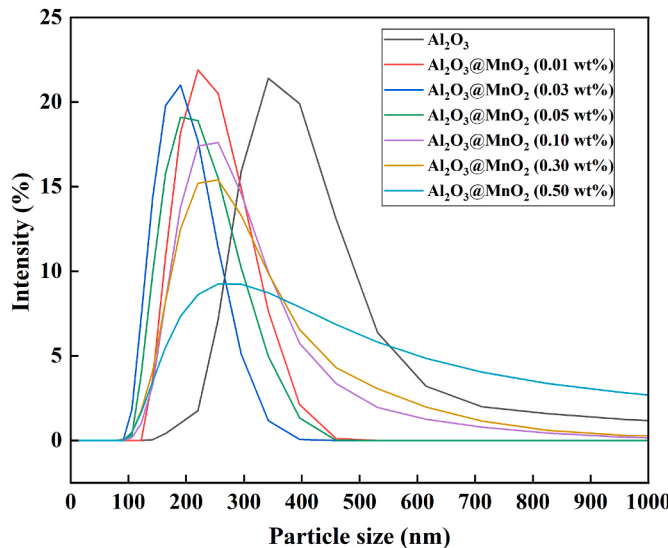


Fig. 3. Size distribution of Al₂O₃ and Al₂O₃@MnO₂ composite abrasive (pH = 2).

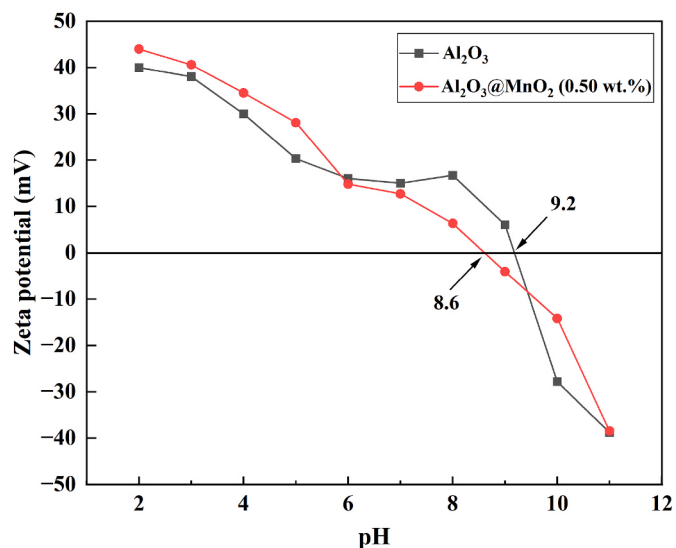


Fig. 4. The zeta potential of Al₂O₃ and Al₂O₃@MnO₂ (0.50 wt%) composite abrasive at different pH values.

absolute value of the zeta potential of composite abrasive is greater than that of pure Al_2O_3 abrasive, indicating that composite abrasive has better dispersion stability under strong acid condition [31]. It can also be seen from Fig. 3 that the particle size of $\text{Al}_2\text{O}_3@\text{MnO}_2$ (0.01–0.30 wt %) composite abrasives is smaller, indicating an enhancement in the agglomeration of pure alumina and increased dispersion stability of $\text{Al}_2\text{O}_3@\text{MnO}_2$ (0.01–0.30 wt%) composite abrasives [32]. On the other hand, adding varying amounts of manganese will result in variable surface properties, and the isoelectric point will change with the change in the surface properties of the abrasive [33]. As shown in Fig. 4, the isoelectric point of Al_2O_3 is 9.2, while that of $\text{Al}_2\text{O}_3@\text{MnO}_2$ (0.50 wt%) is 8.6. Compared with pure Al_2O_3 abrasive, the isoelectric point shifts towards lower pH values, which may be connected to an increase in Mn^{4+} concentration. Consistent with the previous testing, the composite abrasive loaded with MnO_2 exhibited superior stability and dispersion in acidic conditions, which is advantageous for subsequent polishing performance experiments.

Based on the above structural and morphological testing, it is evident that MnO_2 is successfully loaded on the external surface of Al_2O_3 , and the $\text{Al}_2\text{O}_3@\text{MnO}_2$ (0.50 wt%) composite abrasive has improved dispersion and stability in acidic conditions.

3.2. CMP performance

Material removal rate (MRR) is one of the crucial metric to evaluate the CMP performance [34]. The enhanced performance of CMP is a result of a synergistic effect of chemical and mechanical actions. Insufficient mechanical action delays the removal of SiC oxide layer, while excessive mechanical action can cause surface defects by creating scratches on SiC surface [11,35]. Therefore, the issue of the balance between chemical and mechanical effects in the CMP process is of utmost importance.

Fig. 5 illustrates the impact of varying MnO_2 content on the MRR of $\text{Al}_2\text{O}_3@\text{MnO}_2$ composite abrasive. The pure Al_2O_3 abrasive is indicated as a reference. The MRR of $\text{Al}_2\text{O}_3@\text{MnO}_2$ composite abrasive initially increases with the increase of MnO_2 content. At the MnO_2 coating amount of 0.05 wt%, the maximum MRR reaches 640.47 nm/h, which is 76% higher than the MRR of pure Al_2O_3 abrasive (364.50 nm/h). At coating amounts exceeding 0.05 wt%, the MRR gradually decreases. According to the variation of MRR, it can be inferred that the oxidation rate may gradually increase in the beginning stage when the coating amount is below 0.05 wt%, and the removal rate of the generated oxide is also gradually increasing. When the coating amount exceeds 0.05 wt %, excessive MnO_2 coating might diminish the mechanical action and

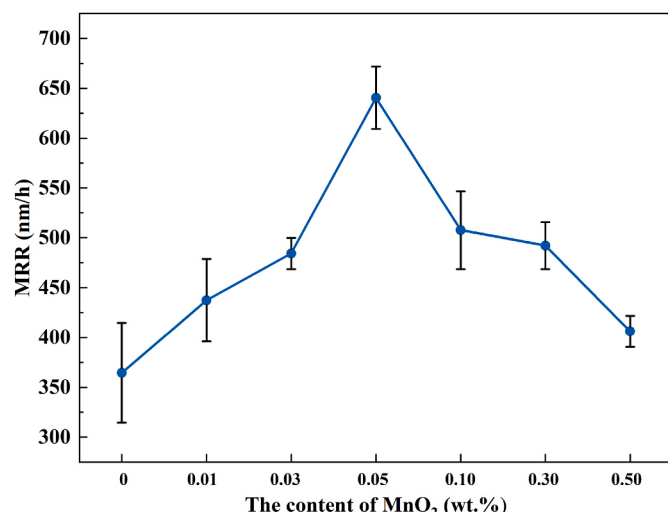


Fig. 5. The effect of MnO_2 coating amounts on MRR.

hardness of composite abrasives. Therefore, the high MRR of SiC was attained and the ideal balance between mechanical and chemical effects was reached at 0.05 wt% MnO_2 coating.

In the process of CMP, it is expected to obtain higher MRR and a surface with less damage at the nanoscale. Therefore, it is necessary to assess the surface roughness of the substrate. Fig. 6 shows the surface profile comparison of SiC in three different environments. SiC substrate in its unpolished state exhibits a surface that is characterized by prominent big pores and a surface roughness of up to 3.31 nm. Polishing SiC surface with Al_2O_3 abrasive resulted in a decrease in surface roughness to 2.70 nm. However, obvious scratches appeared on SiC surface. After polishing with $\text{Al}_2\text{O}_3@\text{MnO}_2$ (0.05 wt%) composite abrasive, the Sa of SiC was effectively decreased to 1.50 nm, and the surface roughness was reduced without obvious scratches and holes. It is possible that the hardness, angular and irregular shape of Al_2O_3 abrasive may produce more mechanical action than chemical activity, leading to visible scratches on the substrate's surface [36]. The Mohs hardness of MnO_2 is lower than that of alumina [37]. Therefore, $\text{Al}_2\text{O}_3@\text{MnO}_2$ (0.05 wt%) composite abrasive can reduce the scratches and improved surface quality of the substrate.

Based on the aforementioned experiments, the best CMP performance is attained when the amount of MnO_2 coating is 0.05 wt%.

3.3. Analysis of the polishing mechanism

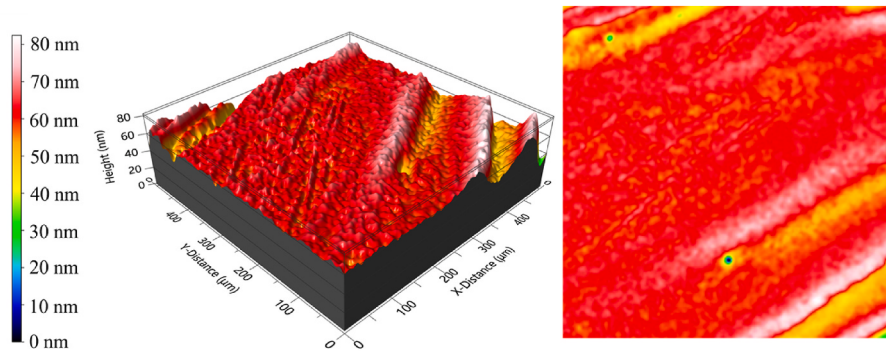
The mechanism of the CMP process is complex, the best performance can be obtained when the chemical and mechanical effects reach the dynamic balance, thus the two aspects are discussed. According to the previous CMP performance test, taking $\text{Al}_2\text{O}_3@\text{MnO}_2$ (0.05 wt%) composite abrasive as an example, the polishing mechanism of MnO_2 coating Al_2O_3 on SiC substrate is analyzed. The oxidation rate plays a crucial role in the process of polishing silicon carbide, as it directly affects the MRR [38]. The oxidation of SiC surface before and after the CMP was analyzed by X-ray photoelectron spectroscopy (XPS), and the results are shown in Fig. 7. Narrow scan spectra of Si 2p and C 1s were obtained (Fig. 8) to further illustrate the degree of oxidation on SiC surface, and manganese was observed on the substrate surface after CMP (Fig. 9).

By comparing the XPS scan full spectrum of 4H-SiC (0001) before and after CMP (Fig. 7), the presence of Mn element is observed in the spectrum after CMP. Curve (a) suggests that new compounds containing Mn element have formed on the surface of SiC. However, further analysis of the specific valence state requires analysis of the narrow scan spectra.

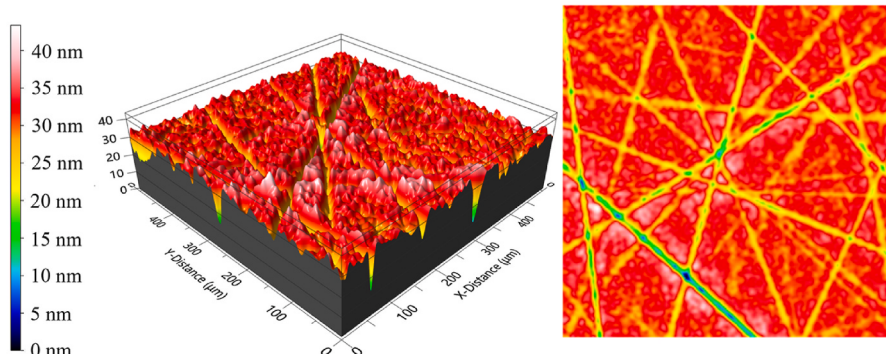
According to the Si 2p spectral analysis of Fig. 8, the binding energies of Si 2p before CMP are 100.1 eV and 102.1 eV, corresponding to Si-C and Si-C-O [9], with higher Si-C peak and lower Si-C-O peak. After CMP, the Si-C binding is significantly reduced, while the Si-C-O intensity is increased, indicating that oxidation reaction may occur on the surface of SiC [39]. In addition, there is a peak of binding energy of 104.3 eV, corresponding to SiO_{x}C_y [40], which is also the oxidation product of SiC. According to the C 1s spectral analysis of Fig. 8, the binding energy of C 1s before CMP is observed at 282.1 eV, 284.9 eV, 286.1 eV, 288.5 eV, corresponding to C-Si, C-C, C-O, and C=O, respectively. The peak of C-C binding energy could be attributed to the adhesion of C substances on the polished SiC surface or the pollution of C-containing substances in the environment [41]. After CMP, the new C-O peak is enhanced, and C-Si oxidation products $\text{Si}_4\text{C}_4\text{O}_4$ (285.1 eV) and $\text{Si}_4\text{C}_{4-x}\text{O}_2$ (282.8 eV) appear on SiC surface [42], further indicating that SiC surface was oxidized.

In addition, Fig. 9 illustrates the appearance of Mn elements on SiC surface in the XPS scan spectrum after CMP. The binding energy of Mn 2p 1/2 and Mn 2p 3/2 is 653.9 eV and 643.4 eV, corresponding to the Mn-O bond in MnO_2 , and the binding energy of 641.9 corresponds to Mn-O-Si bond [43,44]. This could be because the MnO_2 in the slurry reacts with the oxidation products of SiC to generate Mn-O-Si bonds. The XPS results reveal the formation of new oxides on the surface of SiC

(a) Sa=3.31 nm



(b) Sa=2.70 nm



(c) Sa=1.50 nm

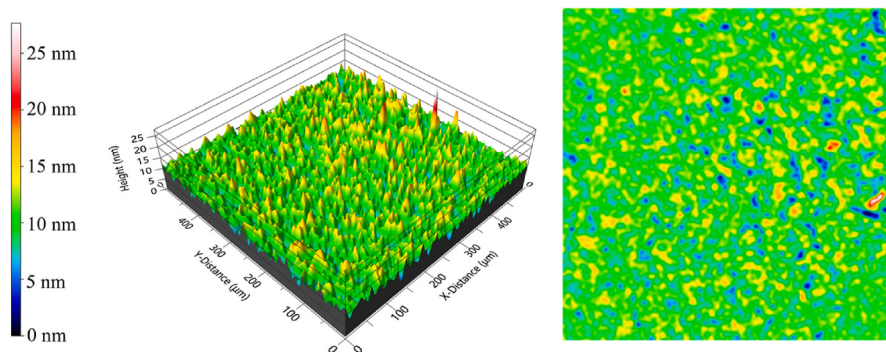


Fig. 6. The 3D and 2D surface profile of SiC: (a) unpolished, $S_a = 3.31$ nm (b) polished by Al_2O_3 , $S_a = 2.70$ nm (c) polished by $\text{Al}_2\text{O}_3@\text{MnO}_2$ (0.05 wt%), $S_a = 1.50$ nm (the measuring area is $500 \mu\text{m} \times 500 \mu\text{m}$, the left scale indicates the range of the z-axis).

after CMP. The surface of SiC polished by Al₂O₃@MnO₂ (0.05 wt%) composite abrasive generates a soft oxide layer, which can be removed easily.

In addition to chemical actions, mechanical actions are also crucial in CMP, and therefore Al₂O₃@MnO₂ composite abrasive needs to be explained in terms of mechanical mechanisms [45]. In this work, contact angle and friction coefficient experiments were used to examine the interaction between the Al₂O₃@MnO₂ composite abrasive and SiC in the CMP experiment.

Fig. 10 illustrates the contact angles of different abrasive with SiC substrate. It can be observed that the maximum contact angle of pure Al₂O₃ abrasive slurry on SiC substrate is 65.90° (Fig. 10a). When the amount of MnO₂ coating is 0.05 wt%, the minimum value of contact angle is 37.45° . The hydrophobicity of SiC makes the initial contact angle larger [15]. After the Al₂O₃ coated with MnO₂, the composite

abrasive becomes soft and prone to elastic deformation. This efficiently expands the contact area with SiC substrate surface and enhances the spreading ability, resulting in a decrease in the contact angle. When the MnO₂ loading is too large, the composite abrasive aggregation leads to the increase of particle size, and the hydrophobicity of the composite abrasive increases, thus the contact area between the abrasive and SiC substrate decreases [28,46,47]. In general, the composite abrasive effectively increases the wettability of the polishing slurry.

On the other hand, the coefficient of dynamic friction is also a research object of mechanical effects. It is shown that the MRR increases with the increase of the dynamic friction coefficient between the abrasive and SiC substrate [48]. In this experiment, the CMP environment during the polishing process was simulated using a dynamic friction coefficient meter. Fig. 11 shows the dynamic friction coefficient between different Al₂O₃@MnO₂ composite abrasive and SiC substrate. The

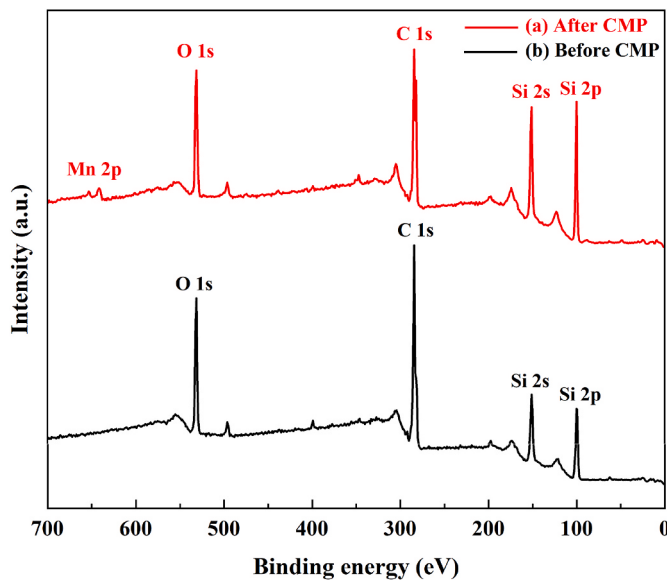


Fig. 7. XPS scan full spectrum of 4H-SiC (0001) (a) after and (b) before CMP.

initial dynamic friction coefficient of pure Al_2O_3 as an abrasive is merely 0.18. However, after MnO_2 coating, the dynamic friction coefficient gradually increased, reaching a maximum value of 0.24. Due to the smaller hardness of MnO_2 , it may be more likely to produce deformation, which increases the contact area between the abrasive and wafer.

Therefore, the dynamic friction coefficient is positively correlated with the mechanical effect. Nevertheless, if the amount of MnO_2 coating is excessive, the aggregation of composite abrasives reduces the amount of effective abrasives, which reduces the MRR [47]. This is similar with the earlier MRR results in CMP performance.

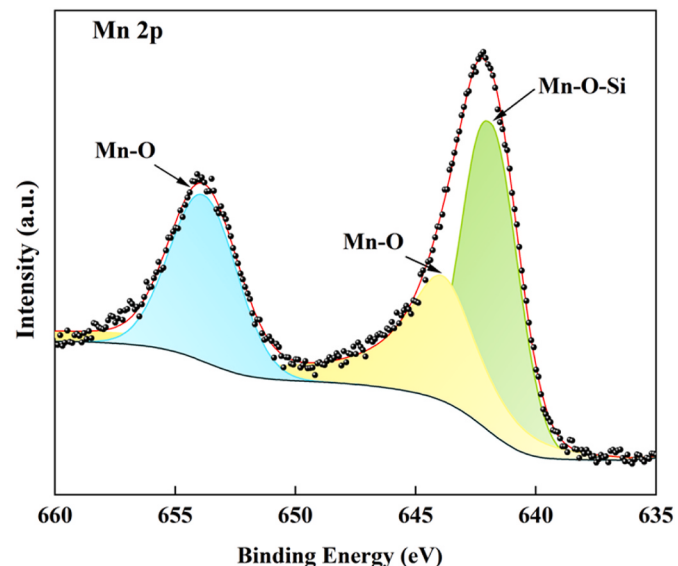


Fig. 9. XPS narrow scan spectrum of Mn 2p.

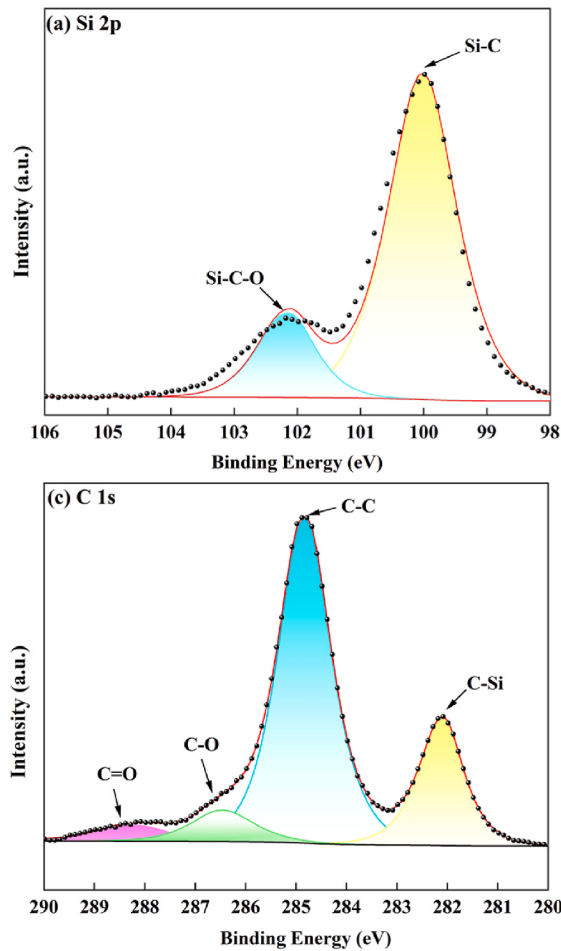


Fig. 8. XPS narrow scan spectrum of Si 2p (a) before CMP (b) after CMP and C1s (c) before CMP (d) after CMP.

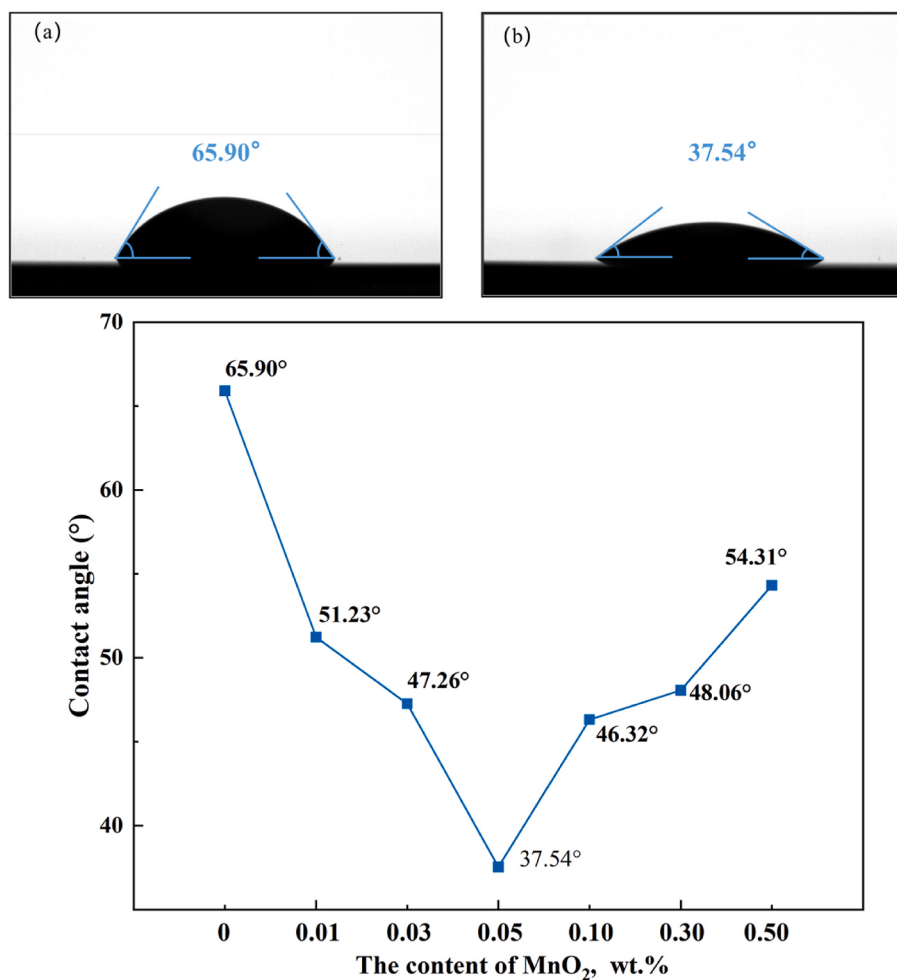


Fig. 10. Contact angle test of $\text{Al}_2\text{O}_3@\text{MnO}_2$ composite abrasive with different MnO_2 coating amounts.

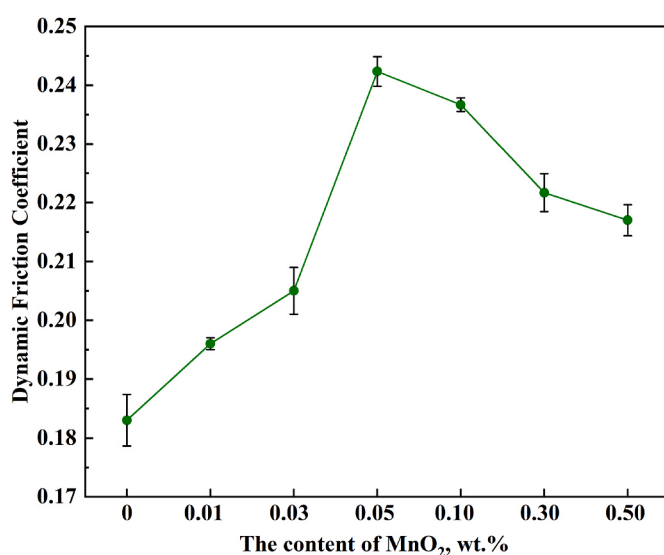


Fig. 11. Dynamic friction coefficient of $\text{Al}_2\text{O}_3@\text{MnO}_2$ composite abrasive slurry.

In order to illustrate the interaction between composite abrasive and SiC substrate more visually, the contact wear model between $\text{Al}_2\text{O}_3@\text{MnO}_2$ (0.05 wt%) composite abrasive and SiC substrate is established in Fig. 12. Under acidic conditions, SiC is oxidized to soft

SiO_2 under the action of KMnO_4 , reacts with the coated MnO_2 to form $\text{Mn}-\text{O}-\text{Si}$ bonds, and is finally removed by the mechanical action of $\text{Al}_2\text{O}_3@\text{MnO}_2$.

4. Conclusion

In this paper, a series of MnO_2 -coated Al_2O_3 composite was prepared, and the coating amount of MnO_2 was changed to study the best CMP performance on SiC substrate. The XRD results show that MnO_2 is successfully coated on the outer surface of Al_2O_3 . SEM and size distribution results show that the addition of MnO_2 improves the dispersibility. Zeta potential analysis results reveal that the $\text{Al}_2\text{O}_3@\text{MnO}_2$ composite abrasive exhibits excellent dispersion stability in acidic conditions. The CMP tests indicate that the best polishing performance is achieved by using the $\text{Al}_2\text{O}_3@\text{MnO}_2$ (0.05 wt%) composite abrasive, which results in a maximum MRR of 640.47 nm/h and minimum Sa of 1.5 nm. By analyzing the polishing mechanism, the surface of SiC is oxidized to SiO_2 after composite abrasive polishing, and the $\text{Mn}-\text{O}-\text{Si}$ bond is formed to accelerate the chemical reaction rate. The $\text{Al}_2\text{O}_3@\text{MnO}_2$ (0.05 wt%) composite abrasive exhibits the lowest contact angle and the highest dynamic friction coefficient on SiC substrate, which enhances the mechanical action in CMP and leads to an improvement in the MRR.

Declaration of competing interest

The authors declare that they have no known competing financial interests or personal relationships that could have appeared to influence

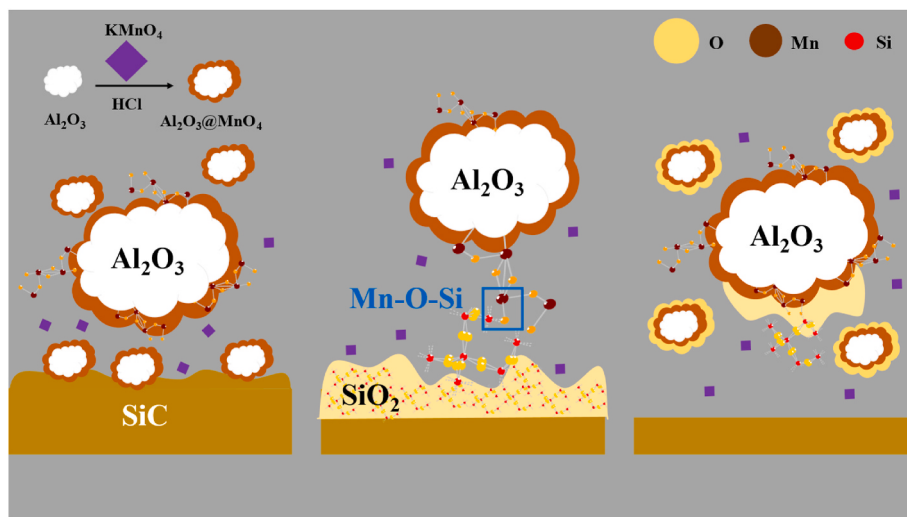


Fig. 12. Contact wear model of $\text{Al}_2\text{O}_3@\text{MnO}_2$ (0.05 wt%) composite abrasive and SiC substrate.

the work reported in this paper.

Acknowledgments

This work was supported by the National Natural Science Foundation of China (Grant Number 51975343), Science and Technology Major Project of Inner Mongolia Autonomous Region in China (No. 2021ZD0028), Shanghai Engineering Research Center for Integrated Circuits and Advanced Display Materials, and Shanghai Technical Service Center for Advanced Ceramics Structure Design and Precision Manufacturing (No. 20DZ2294000).

J.

References

- [1] L. Han, L. Liang, Y. Kang, Y. Qiu, A review of SiC IGBT: models, fabrications, characteristics, and applications, *IEEE Trans. Power Electron.* 36 (2021) 2093, <https://doi.org/10.1109/tpe.2020.3005940>.
- [2] H. Hara, Y. Sano, H. Mimura, K. Arima, A. Kubota, K. Yagi, J. Murata, K. Yamauchi, Novel abrasive-free planarization of 4H-SiC (0001) using catalyst, *J. Electron. Mater.* 35 (2006) L11–L14, <https://doi.org/10.1007/s11664-006-0218-6>.
- [3] Q. Zhao, S. Xie, H. Wang, L. Yang, X. Mei, Y. He, Synergistic effect of aminosilane and K_2CO_3 on improving Chemical Mechanical Polishing performance of SiO_2 dielectric layer, *Mater. Sci. Semicond. Process.* 146 (2022), <https://doi.org/10.1016/j.mssp.2022.106702>.
- [4] C.H. Hsieh, C.Y. Chang, Y.K. Hsiao, C.C.A. Chen, C.C. Tu, H.C. Kuo, Recent advances in silicon carbide chemical mechanical polishing technologies, *Micro* (2022) 13, <https://doi.org/10.3390/mi3101752>.
- [5] H. Aida, T. Doi, H. Takeda, H. Katakura, S.-W. Kim, K. Koyama, T. Yamazaki, M. Ueda, Ultraprecision CMP for sapphire, GaN, and SiC for advanced optoelectronics materials, *Curr. Appl. Phys.* 12 (2012) S41–S46, <https://doi.org/10.1016/j.cap.2012.02.016>.
- [6] Y. Zhou, G. Pan, X. Shi, L. Xu, C. Zou, H. Gong, G. Luo, XPS, UV-vis spectroscopy and AFM studies on removal mechanisms of Si-face SiC wafer chemical mechanical polishing (CMP), *Appl. Surf. Sci.* 316 (2014) 643–648, <https://doi.org/10.1016/j.apsusc.2014.08.011>.
- [7] Z. Ni, G. Chen, L. Xu, Y. Bai, Q. Li, Y. Zhao, Effects of different oxidants on 6H-SiC chemical-mechanical polishing, *Jour. of Mech. Eng.* 54 (2018) 224–231, <https://doi.org/10.3901/JME.2018.19.224>.
- [8] G. Chen, Z. Ni, L. Xu, Q. Li, Y. Zhao, Performance of colloidal silica and ceria based slurries on CMP of Si-face 6H-SiC substrates, *Appl. Surf. Sci.* 359 (2015) 664–668, <https://doi.org/10.1016/j.apsusc.2015.10.158>.
- [9] W. Wang, W. Liu, Z. Song, Y. Xu, Effect of ferric nitrate on semi-insulating 4H-SiC (0001) chemical mechanical polishing, *ECS J. Solid State Sci. Technol.* 11 (2022), <https://doi.org/10.1149/2162-8777/ac7bef>.
- [10] P. Zhao, T. Yin, T. Doi, S. Kurokawa, K. Seshimo, D. Ye, J. Cai, Effect of Mn-based slurries on chemical mechanical polishing of SiC substrates, *ECS J. Solid State Sci. Technol.* 11 (2022), <https://doi.org/10.1149/2162-8777/ac7bef>.
- [11] W. Wang, X. Lu, X. Wu, Y. Zhang, R. Wang, D. Yang, X. Pi, Chemical-mechanical polishing of 4H silicon carbide wafers, *Adv. Mater. Interfac.* 10 (2023), <https://doi.org/10.1002/admi.202202369>.
- [12] L. Zhou, V. Audurier, P. Pirouz, J.A. Powell, Chemomechanical polishing of silicon carbide, *J. Electrochem. Soc.* 144 (1997) L161–L163, <https://doi.org/10.1149/1.1837711>.
- [13] S. Huang, X. Li, D. Mu, C. Cui, H. Huang, H. Huang, Polishing performance and mechanism of a water-based nanosuspension using diamond particles and GO nanosheets as additives, *Tribol. Int.* 164 (2021), <https://doi.org/10.1016/j.triboint.2021.107241>.
- [14] J. Su, J. Du, L. Ma, Z. Zhang, R. Kang, Material removal rate of 6H-SiC crystal substrate CMP using an alumina (Al_2O_3) abrasive, *J. Semiconduct.* 33 (2012), <https://doi.org/10.1088/1674-4926/33/10/106003>, 106003-106003-106007.
- [15] W. Wang, B. Zhang, Y. Shi, D. Zhou, R. Wang, Improvement in dispersion stability of alumina suspensions and corresponding chemical mechanical polishing performance, *Appl. Surf. Sci.* 597 (2022), <https://doi.org/10.1016/j.apsusc.2022.153703>.
- [16] T. Li, H. Sun, D. Wang, J. Huang, D. Li, F. Lei, D. Sun, High-performance chemical mechanical polishing slurry for aluminum alloy using hybrid abrasives of zirconium phosphate and alumina, *Appl. Surf. Sci.* 537 (2021), <https://doi.org/10.1016/j.apsusc.2020.147859>.
- [17] L. Geerts, H. Geerts-Claes, A. Skorikov, J. Vermeersch, G. Vanbutsele, V. Galvita, D. Constales, C.V. Chandran, S. Radhakrishnan, J.W. Seo, E. Breynaert, S. Bals, S. P. Sree, J.A. Martens, Spherical core-shell alumina support particles for model platinum catalysts, *Nanoscale* 13 (2021) 4221–4232, <https://doi.org/10.1039/donr08456e>.
- [18] H. Lei, P. Zhang, Preparation of alumina/silica core-shell abrasives and their CMP behavior, *Appl. Surf. Sci.* 253 (2007) 8754–8761, <https://doi.org/10.1016/j.apsusc.2007.04.079>.
- [19] X. Wang, H. Lei, R. Chen, CMP behavior of alumina/metatitanic acid core-shell abrasives on sapphire substrates, *Precis. Eng.* 50 (2017) 263–268, <https://doi.org/10.1016/j.precisioneng.2017.05.013>.
- [20] Z. Zhang, Z. Jin, J. Guo, The effect of the interface reaction mode on chemical mechanical polishing, *CIRP Ann. - Manuf. Technol.* 31 (2020) 539–547, <https://doi.org/10.1016/j.cirpj.2020.08.005>.
- [21] X. Yuan, C. Chen, H. Lei, Z. Zhang, Synthesis, characterization of $\text{CeO}_2@\text{ZIF}-8$ composite abrasives and their chemical mechanical polishing behavior on glass substrate, *Ceram. Int.* 49 (2023) 5189–5198, <https://doi.org/10.1016/j.ceramint.2022.10.037>.
- [22] S. Kurokawa, T. Doi, O. Ohnishi, T. Yamazaki, Z. Tan, T. Yin, Characteristics in SiC-CMP using MnO_2 slurry with strong oxidant under different atmospheric conditions, *MRS 1560* (2013), <https://doi.org/10.1557/opl.2013.903>.
- [23] T. Yin, T. Doi, S. Kurokawa, Z.Z. Zhou, K.P. Feng, Polishing characteristics of MnO_2 polishing slurry on the Si-face of SiC wafer, *Int. J. Precis. Eng. Manuf.* 19 (2018) 1773–1780, <https://doi.org/10.1007/s12541-018-0206-9>.
- [24] L. Miao, J.L. Wang, P.Y. Zhang, Review on manganese dioxide for catalytic oxidation of airborne formaldehyde, *Appl. Surf. Sci.* 466 (2019) 441–453, <https://doi.org/10.1016/j.apsusc.2018.10.031>.
- [25] J. Jia, P. Zhang, L. Chen, The effect of morphology of $\alpha\text{-MnO}_2$ on catalytic decomposition of gaseous ozone, *Catal. Sci. Technol.* 6 (2016) 5841–5847, <https://doi.org/10.1039/c6cy00301j>.
- [26] S. Lin, Y. Yu, M. Zhong, H. Yang, C. Zhang, Z. Zhang, W. Xu, J. Xie, Y. Qiu, The activation mechanism of oxalic acid on γ -alumina and the formation of α -alumina, *Ceram. Int.* 47 (2021) 26869–26876, <https://doi.org/10.1016/j.ceramint.2021.06.096>.
- [27] S. Biswas, A. Pal, Visible light assisted Fenton type degradation of methylene blue by admicelle anchored alumina supported rod shaped manganese oxide, *J. Water Process Eng.* 36 (2020), <https://doi.org/10.1016/j.jwpe.2020.101272>.
- [28] W. Zhang, H. Lei, W. Liu, Z. Zhang, Effect of the carboxyl group number of the complexing agent on polishing performance of alumina slurry in sapphire CMP,

- Ceram. Int. 49 (2023) 13687–13697, <https://doi.org/10.1016/j.ceramint.2022.12.246>.
- [29] Z. Zhang, L. Yu, W. Liu, Z. Song, Surface modification of ceria nanoparticles and their chemical mechanical polishing behavior on glass substrate, Appl. Surf. Sci. 256 (2010) 3856–3861, <https://doi.org/10.1016/j.apsusc.2010.01.040>.
- [30] B.P. Singh, S. Bhattacharjee, L. Besra, D.K. Sengupta, Evaluation of dispersibility of aqueous alumina suspension in presence of Darvan C, Ceram. Int. 30 (2004) 939–946, <https://doi.org/10.1016/j.ceramint.2003.11.007>.
- [31] N. Zeng, H. Zhao, Y. Liu, C. Wang, C. Luo, W. Wang, T. Ma, Optimizing of the colloidal dispersity of silica nanoparticle slurries for chemical mechanical polishing, Silicon 14 (2022) 7473–7481, <https://doi.org/10.1007/s12633-021-01448-y>.
- [32] R. Ding, H. Lei, C. Chen, Z. Zhang, Preparation of the nanodiamond@SiO₂ abrasive and its effect on the polishing performance of zirconia Ceramics, ECS J. Solid State Sci. Technol. 11 (2022), <https://doi.org/10.1149/2162-8777/ac757e>.
- [33] I. Vazquez-Garrido, A. Lopez-Benitez, A. Guevara-Lara, G. Berhault, Synthesis of NiMo catalysts supported on Mn-Al2O3 for obtaining green diesel from waste soybean oil, Catal. Today 365 (2021) 327–340, <https://doi.org/10.1016/j.cattod.2020.06.001>.
- [34] J. Zhang, Y. Jiang, H. Luo, S. Yin, Prediction of material removal rate in chemical mechanical polishing via residual convolutional neural network, Control Eng. Pract. 107 (2021), <https://doi.org/10.1016/j.conengprac.2020.104673>.
- [35] D. Lee, H.S. Lee, H. Jeong, Slurry components in metal chemical mechanical planarization (CMP) process: a review, Int. J. Precis. Eng. Manuf. 17 (2016) 1751–1762, <https://doi.org/10.1007/s12541-016-0201-y>.
- [36] G. Chen, J. Li, J. Long, H. Luo, Y. Zhou, X. Xie, G. Pan, Surface modulation to enhance chemical mechanical polishing performance of sliced silicon carbide Si-face, Appl. Surf. Sci. 536 (2021), <https://doi.org/10.1016/j.apsusc.2020.147963>.
- [37] Y. Chen, H. Cong, Y. Shen, B. Yu, Biomedical application of manganese dioxide nanomaterials, Nanotechnology 31 (2020), <https://doi.org/10.1088/1361-6528/ab6fe1>.
- [38] C.-H. Hsieh, C.-Y. Chang, Y.-K. Hsiao, C.-C.A. Chen, C.-C. Tu, H.-C. Kuo, Recent advances in silicon carbide chemical mechanical polishing technologies, Micromachines 13 (2022), <https://doi.org/10.3390/mi13101752>.
- [39] G.P. Chen, J.G. Li, J.Y. Long, H.M. Luo, Y. Zhou, X.Z. Xie, G.S. Pan, Surface modulation to enhance chemical mechanical polishing performance of sliced silicon carbide Si-face, Appl. Surf. Sci. 536 (2021), <https://doi.org/10.1016/j.apsusc.2020.147963>.
- [40] B. Gao, D. Guo, X. Zhang, G. Chen, G. Pan, Picosecond laser-assisted chemical mechanical polishing (CMP): aiming at the Si-face of single-crystal 6H-SiC wafer, ECS J. Solid State Sci. Technol. 10 (2021), <https://doi.org/10.1149/2162-8777/acb726>.
- [41] K. Yamamura, T. Takiguchi, M. Ueda, H. Deng, A.N. Hattori, N. Zettsu, Plasma assisted polishing of single crystal SiC for obtaining atomically flat strain-free surface, CIRP Ann. - Manuf. Technol. 60 (2011) 571–574, <https://doi.org/10.1016/j.cirp.2011.03.072>.
- [42] P. Zhao, E. Rusli, J. Xia, C. Tan, Y. Liu, C.-C. Tin, S. Yoon, W. Zhu, J. Ahn, Study of carbon in thermal oxide formed on 4H-SiC by XPS, Mater. Sci. Found. 656 (2005) 483–485, <https://doi.org/10.4028/www.scientific.net/MSF.483-485.653>.
- [43] B.J. Tan, K.J. Klabunde, P.M.A. Sherwood, X-ray photoelectron spectroscopy studies of solvated metal atom dispersed catalysts. Monometallic iron and bimetallic iron-cobalt particles on alumina, Chem. Mater. 2 (1990) 191, <https://doi.org/10.1021/cm00008a021>.
- [44] A.P. Grosvenor, E.M. Bellhouse, A. Korinek, M. Bugnet, J.R. McDermid, XPS and EELS characterization of Mn₂SiO₄, MnSiO₃ and MnAl₂O₄, Appl. Surf. Sci. 379 (2016) 242–248, <https://doi.org/10.1016/j.apsusc.2016.03.235>.
- [45] Q. Mu, Z. Jin, X. Han, Y. Yan, Z. Zhang, P. Zhou, Effects of slurry pH on chemical and mechanical actions during chemical mechanical polishing of YAG, Appl. Surf. Sci. 563 (2021), <https://doi.org/10.1016/j.apsusc.2021.150359>.
- [46] Y. Dong, H. Lei, W. Liu, Y. Chen, Preparation of ellipsoidal rod-shaped silica nanocomposite abrasives by Chromium ion/PEG200 induced method for sapphire substrates chemical mechanical polishing, J. Alloys Compd. 777 (2019) 1294–1303, <https://doi.org/10.1016/j.jallcom.2018.11.080>.
- [47] R. Ding, H. Lei, C. Chen, Z. Zhang, Preparation of the nanodiamond@SiO₂ abrasive and its effect on the polishing performance of zirconia Ceramics, Ecs J. Solid State Sci. Tech. 11 (2022), <https://doi.org/10.1149/2162-8777/ac757e>.
- [48] Y. Wang, Y. Chen, F. Qi, D. Zhao, W. Liu, A material removal model for silicon oxide layers in chemical mechanical planarization considering the promoted chemical reaction by the down pressure, Tribol. Int. 93 (2016) 11–16, <https://doi.org/10.1016/j.triboint.2015.09.008>.